Research Article

Fuzhang Wang, Muhammad Sohail*, Umar Nazir*, Essam R. El-Zahar, Choonkil Park*, and Noman Jabbar

An implication of magnetic dipole in Carreau Yasuda liquid influenced by engine oil using ternary hybrid nanomaterial

https://doi.org/10.1515/ntrev-2022-0100
received January 5, 2022; accepted March 19, 2022

Abstract: The aim of this work was to study the enhancement of thermal transportation in Carreau Yasuda liquid passed over a vertical surface in the presence of magnetic dipole. A mixture of tri-hybrid nanoparticles (Al_2O_3, MoS_3, TiO_3) is inserted into the Carreau Yasuda liquid. The transport phenomenon of heat is derived in the presence of heat source/sink contribution. The concept boundary layer theory is engaged to derive the mathematical expression for momentum and energy in the form of coupled partial differential equations. The derivations are transformed into a set of coupled nonlinear ordinary differential equations (ODEs) with the help of suitable similarity transformation. These converted ODEs have been handled numerically *via* finite element method. The grid-independent analysis is established for 300 elements. The impact of numerous involved parameters on temperature and velocity solution is plotted and their contribution is recorded. Temperature profile is inclined versus the higher values of heat generation and viscous dissipation numbers while thermal layers are also increasing the behavior. A vital role of magnetic dipole is examined to raise the production of thermal layers but declination is noticed in flow profile.

Keywords: magnetic dipole, Carreau Yasuda liquid, ternary hybrid nanofluid, thermal performance, engine oil, heat source sink, vertical surface

*** Corresponding author: Muhammad Sohail,** Department of Mathematics, Khwaja Fareed University of Engineering & Information Technology, Rahim Yar Khan 64200, Pakistan, e-mail: muhammad_sohail111@yahoo.com
*** Corresponding author: Umar Nazir,** Department of Applied Mathematics and Statistics, Institute of Space Technology, P.O. Box 2750, Islamabad 44000, Pakistan, e-mail: nazir_u2563@yahoo.com
*** Corresponding author: Choonkil Park,** Research Institute for Natural Sciences, Hanyang University, Seoul 04763, Republic of Korea, e-mail: baak@hanyang.ac.kr
Fuzhang Wang: Nanchang Institute of Technology, Nanchang 330044, China; School of Mathematics and Statistics, Xuzhou University of Technology, Xuzhou 221018, China
Essam R. El-Zahar: Department of Mathematics, College of Science and Humanities in Al-Kharj, Prince Sattam bin Abdulaziz University, P.O. Box 83, Al-Kharj 11942, Saudi Arabia; Department of Basic Engineering Science, Faculty of Engineering, Menoufia University, Shebin El-Kom 32511, Egypt
Noman Jabbar: Department of Applied Mathematics and Statistics, Institute of Space Technology, P.O. Box 2750, Islamabad 44000, Pakistan

Nomenclature

$v,\ u$	velocity components
ρ	fluid density
μ_0	magnetic permeability
H	magnetic field
Λ	Carreau Yasuda number
C_p	specific heat
Q_0	heat source number
T	fluid temperature
u_e	free stream velocity
β	ferrohydrodynamic interaction number
π	Pi
H_b	component of magnetic field
We	Weissenberg number
λ	viscous dissipation number
$\varphi_3,\ \varphi_1,\ \varphi_3$	volume fractions
σ	electrical conductivity
Re	Reynolds number
$a,\ b$	space coordinates
P	pressure
M	magnetization
γ	strength of the magnetic dipole
d	fluid number
k	thermal conductivity
S_1	stretching ratio number
T_w	wall temperature
ψ	trial shape function

H_a	component of magnetic field
Thnf, f, bf	ternary hybrid nanofluid, fluid and base fluid
m	power law number
Pr	Prandtl number
ϵ	ratio parameter
H_t	heat source number
Nu	Nusselt number
w_3, w_2, w_1	weight functions

1 Introduction

Numerous research works have been carried out on nanomaterials due to their wider applications in medicine, energy system and different industrial mechanisms. The involvement of nanoparticles has also been tested for the treatment of cancer. Researchers used these nanoparticle mixtures in different liquids to study the thermal performance. For instance, Shah *et al.* [1] worked on ecosystem by studying the inclusion of titanium dioxide particles. Khan *et al.* [2] examined the contribution of slip effects on Eyring–Powell liquid with heat transport in which graphene particles are mixed. The phenomenon of thin film is further discussed under time-dependent magnetic field. The flow-governing equations have been solved analytically *via* homotopic solution scheme. They noted the decline in temperature field against Prandtl number. Rehman *et al.* [3] numerically solved the magnetized non-Newtonian Casson model passed over a radial rotating stretching sheet. They handled the derived boundary layer transformed nonlinear set of differential equations *via* shooting scheme. They observed the decline in fluid velocity by mounting the values of slip parameter, Casson fluid parameter and magnetic parameter. Alobaid *et al.* [4] presented the experimental study of carbon-based nanoparticles to examine the degraded soil properties. Ali *et al.* [5] presented the involvement of thermal radiation and heat generation for the stagnation point flow of viscous liquid past over a stretching cylinder by including the involvement of Brownian motion and thermophoresis. They used shooting scheme to solve the coupled nonlinear ordinary differential equations (ODEs) in unbounded domain. They recorded the decline in velocity against the mounting values of curvature parameter and also the decrease in temperature field is monitored against Prandtl number and radiation parameter. Boarescu *et al.* [6] scrutinized the involvement of nanomaterials in making the different medicines and drugs. Pop *et al.* [7] presented the experimental survey by considering the involvement of nanoparticles in nerve injury treatment. Iacoviță *et al.* [8] examined the involvement of silica nanoparticles to study the cancer cells in human body. Swain *et al.* [9] studied MWCNT/Fe_3O_4 hybrid nanofluid past over an exponentially stretched porous sheet under slip boundary conditions and chemical reaction. They considered the influence of radiation and heat generations in energy equation. They solved the system of nonlinear transformed ODEs *via* BVP4C procedure in MATLAB computational package. They noticed the decrease in velocity, temperature and concentration fields against slip parameter. Furthermore, they monitored the enhancement in heat transfer rate against Prandtl number. Gul and Firdous [10] presented the experimental, theoretical and analytical investigation to discuss the comportment of graphene nanoparticles in water and the flow is produced due to the rotation of disks. They presented the convergence and error analysis. They have shown the rise in fluid velocity against Reynolds number. Tassaddiq *et al.* [11] studied the hybrid nanofluid flow between rotating disks and established the analytical solution. They have considered the involvement of viscous dissipation in energy equation. They noticed the decline in velocity for magnetic parameter. Also, they observed that against volume fraction, temperature field increases but concentration profile decreases. Shafiq *et al.* [12] studied bio-convective and buoyancy-driven flow phenomena for second-grade liquid with chemical reaction. They solved the resulting equations numerically. They noticed the enhancement in motile density profile against thermophoresis parameter, whereas reverse behavior is recorded for Pecklet number. Nisar *et al.* [13] studied the inclusion of gold nanoparticles in micro-polar liquid past over a stretched sheet. They computed the numerical solution for coupled nonlinear transformed ODEs. Khan *et al.* [14] examined the involvement of nanoparticles in bio-convective flow of modified second-grade liquid. They used shooting approach to solve the transformed modeled ODEs. They found the decrease in motile density profile against Lewis number. Waqas *et al.* [15] studied numerically the flow of nanoparticles past over a slandering surface under radiation effect. Some important contributions are reported in refs [16–19] and references therein. Sadat *et al.* [20] performed the model based on 3D Euler equations using invariant solution and lie symmetry study in view of incompressible flow *via* cylindrical coordinates. Mousa *et al.* [21] investigated MHD convection in square cavities using localized heating approach. Ali *et al.* [22] used a new wavelet approach to solve boundary value problems based on adiabatic tubular chemical reactor theory. Sabir *et al.* [23] simulated fourth-order nonlinear system using Levenberg–Marquardt backpropagation approach. Baleanu *et al.* [24] studied the role of nanoparticles containing carbon nanotubes in base fluid called engine oil toward a rotating disc. Khan *et al.* [25] captured the features of activation energy in non-Newtonian liquid considering nanoparticles in the presence of chemical reaction. Khan *et al.* [26] discussed the thermal performance of heat energy using non-Fourier's theory in Williamson liquid containing nanoparticles in the presence of slip conditions toward a porous medium. Khan *et al.* [27] simulated numerical consequences of ferro-fluid using slip conditions in the presence of Darcy–Forchheimer law over a porous surface. Khan *et al.* [28] derived a mathematical model in terms of hyperbolic tangent liquid involving consequences of heat energy and mass diffusion *via* chemical reaction. Hayat *et al.* [29] investigated energy transfer model using the role of thermal radiation in heated cylinder. They simulated a numerical study of various parameters on heat energy and flow. Khan *et al.* [30] discussed consequences of heat energy in second-grade liquid using activation energy in heated channel. Wang *et al.* [31] studied the numerical aspects of energy in Oldroyd-B liquid under action of thermal radiation involving homogeneous–heterogeneous considering heat generation. Qayyum *et al.* [32] developed a model related to five nanoparticles into base fluid using Joule heating considering slip conditions in heated disc. Hayat *et al.* [33] studied consequences based on ferromagnetic-containing nanoparticles in Maxwell fluid. Bhatti *et al.* [34] derived consequences of fluid particle motion and energy transfer in heated asymmetric tapered channel. Bhatti and Abdelsalam [35] captured the features of thermodynamic entropy analysis in Ree–Eyring liquid using irreversibility process. Elkoumy *et al.* [36] studied the aspects of magnetic field in Maxwell fluid in the presence of Hall effects over a porous surface. Abdelsalam *et al.* [37] studied the role of electro-magnetivity in swimming sperms using cervical canal. Eldesoky *et al.* [38] investigated thermal performance in conjunction using slip conditions *via* catheterized pipe. Bhatti *et al.* [39] derived consequences of hybrid nanoparticles to enhance thermal energy effect under the action of magnetic field. Mekheimer *et al.* [40] investigated the thermal performance of nanoparticles in drug delivery and blood hemodynamics. Kalaivanan *et al.* [41] derived the thermal aspects of activation energy and elastic deformation in second-grade liquid inserting nanoparticles. Ganesh *et al.* [42] simulated numerical consequences of energy transfer in Newtonian liquid using conditions of thermal slip in porous surface. Ganesh *et al.* [43] performed model of Casson liquid containing carbon nanotube nanofluid in heated wavy enclosure involving thermal radiations. Ganesh *et al.* [44] studied the performance of nanofluid in Casson material in the presence of Buoyancy-driven convection in parallel hot/cold fins. Ganesh *et al.* [45] investigated the impacts of second-grade liquid inserting nanoparticles in the occurrence of activation energy in a catalytic surface.

An extensive research has been conducted on nanoparticles so far due to their wider applications and utilization. This research is conducted in the presence of magnetic dipole for the inclusion of ternary hybrid nanoparticle mixture in Carreau Yasuda liquid, and numerical computation is performed by using finite element method (FEM) tool in MAPLE18.0 package. The influence of different emerging parameters has been displayed and discussed.

2 Mathematical analysis

A 2D heat transfer model is carried out in Carreau Yasuda liquid past a stretching surface. A Carreau Yasuda liquid is immersed along with base fluid based on engine oil. Three kinds of nanoparticles (aluminum oxide, MoS_2 and TiO_2) are inserted into base liquid as shown in Figure 1. A wall is considered as stretchable to bring motion into fluid particles. A magnetic dipole is considered while the center related to magnetic dipole is placed at the horizontal direction. The flow development is assumed by Figure 2. Transfer of heat energy is considered as absorption and generation into fluid particles. A set of partial differential equations [46,47] is modeled using considerations.

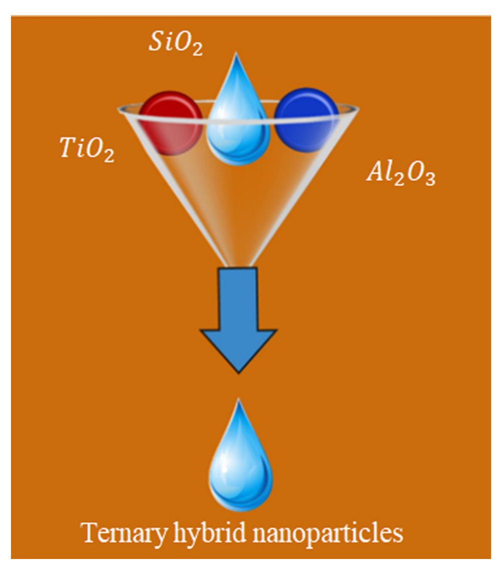

Figure 1: Mixture of nanoparticles resulting in tri-hybrid nanoparticles.

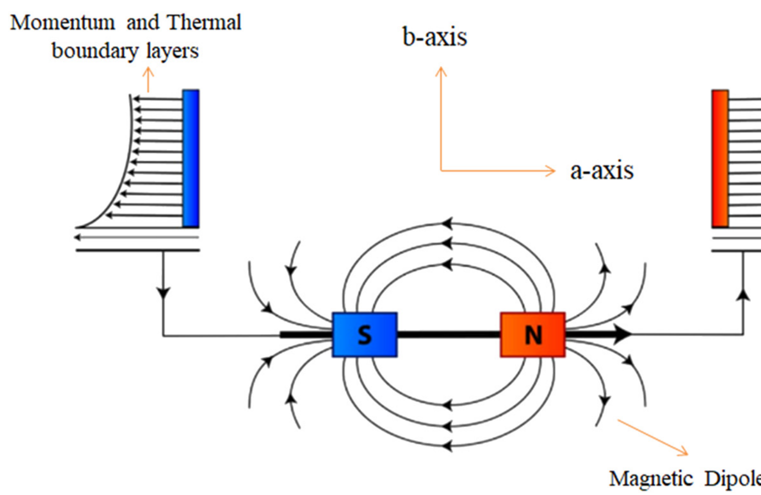

Figure 2: Geometry of developed model.

$$\frac{\partial u}{\partial a}+\frac{\partial v}{\partial b}=0, \tag{1}$$

$$\begin{aligned}&\rho_{\mathrm{Thnf}}\left(u\frac{\partial u}{\partial a}+v\frac{\partial u}{\partial b}\right)\\&=-\frac{\partial P}{\partial a}+\mu_0 M\frac{\partial H}{\partial a}\\&+v_{\mathrm{hnf}}\left[\frac{\partial^2 u}{\partial b^2}+(\Lambda)^d\left(\frac{m-1}{d}\right)(d+1)\frac{\partial^2 u}{\partial b^2}\left(\frac{\partial u}{\partial b}\right)^d\right],\end{aligned} \tag{2}$$

$$\begin{aligned}&(\rho C_{\mathrm{p}})_{\mathrm{Thnf}}\left(u\frac{\partial T}{\partial a}+v\frac{\partial T}{\partial b}\right)+\left(u\frac{\partial H}{\partial a}+v\frac{\partial H}{\partial b}\right)\mu_0 T\frac{\partial M}{\partial T}\\&=K_{\mathrm{Thnf}}\frac{\partial^2 T}{\partial b^2}+Q_0(T-T_\infty).\end{aligned} \tag{3}$$

Figure 2 captures the behavior of developed model. It is mentioned that horizontal surface is assumed where a-axis is taken along the horizontal direction and b-axis is considered along the vertical direction. The motion into fluidic particles is produced using movement of wall. Moreover, direction of magnetic dipole is visualized along a-axis due to an implication of magnetic dipole. Boundary conditions [46,47] are

$$u=sa,\ v=0,\ T=T_w, u=0,\ T\to T_\infty. \tag{4}$$

Required scalar potential *via* magnetic field [46,47] is given as

$$\beta=\frac{\delta}{2\pi}\left(\frac{a}{a^2+(b+d)^2}\right). \tag{5}$$

Components of magnetic inductions are

$$H_a=-\frac{\partial\delta}{\partial a}=\frac{\delta}{2\pi}\left(\frac{a-(b+d)^2}{\{a^2+(b+d)^2\}^2}\right), \tag{6}$$

$$H_b=-\frac{\partial\delta}{\partial b}=\frac{\delta}{2\pi}\left(\frac{2a(b+d)}{\{a^2+(b+d)^2\}^2}\right). \tag{7}$$

Magnitude of magnetic induction is

$$H=\left(\left(\frac{\partial\delta}{\partial b}\right)^2+\left(\frac{\partial\delta}{\partial a}\right)^2\right)^{12}. \tag{8}$$

Using Binomial series and expanding it up to a^2,

$$\begin{aligned}H_b&=\frac{\partial\delta}{\partial b}\left[-\frac{2}{(b+d)^3}+\frac{4a^2}{(b+d)^5}\right],\\H_a&=\frac{\partial\delta}{\partial b}\left[-\frac{2a}{(b+d)^4}\right].\end{aligned} \tag{9}$$

Transformations [46,47] are defined as

$$u=saf',\ v=-(sv_f)^{\frac{1}{2}}f,\ \theta=\frac{T_\infty-T}{T_\infty-T_w},\ \eta=b\left(\frac{s}{b}\right)^{\frac{1}{2}}. \tag{10}$$

A set of dimensionless ODEs with boundary conditions [46,47] is derived as (Table 1)

$$\left.\begin{aligned}&f'''+(\mathrm{We})^d\frac{(m-1)(d+1)}{d}f'''(f'')^d\\&-\frac{v_{\mathrm{Thnf}}}{v_f}\left[f'f'-ff''+\frac{\theta\rho_f 2\beta}{(\eta+\gamma)^4}\right]\\&f'(0)=1,\ f'(\infty)=0,\ f(0)=0,\end{aligned}\right\}, \tag{11}$$

$$\left.\begin{aligned}&\theta''+\frac{(\rho C_{\mathrm{p}})_{\mathrm{Thnf}}k_f}{(\rho C_{\mathrm{p}})_f k_{\mathrm{Thnf}}}\mathrm{Pr}[f\theta'-2f'\theta]+\frac{(\rho C_{\mathrm{p}})_{\mathrm{Thnf}}k_f}{(\rho C_{\mathrm{p}})_f k_{\mathrm{Thnf}}}\frac{\lambda 2\beta f(\theta-\epsilon)}{(\eta+\gamma)^3}\\&-\frac{k_f}{k_{\mathrm{Thnf}}}\frac{4\lambda(1-\phi_2)^{-2.5}}{(1-\phi_1)^{2.5}(1-\phi_3)^{2.5}}(f'')^2+\frac{k_f}{k_{\mathrm{Thnf}}}\mathrm{Pr}H_t\theta=0,\\&\theta(0)=1,\ \theta(\infty)=0.\end{aligned}\right\} \tag{12}$$

Table 1: Thermal properties of hybrid nanoparticles with base fluid [48,49]

	k	σ	ρ
Engine oil	0.144	0.125×10^{-11}	884
Aluminum oxide	32.9	5.96×10^{7}	6,310
Titanium dioxide	8.953	2.4×10^{6}	4,250
Silicon dioxide	1.4013	3.5×10^{6}	2,270

It is noticed that Eqs. (11)–(12) are known as non-Newtonian model in the presence of occurrence of Carreau Yasuda liquid. The present non-Newtonian study is reduced into a case of Newtonian model considering We = 0 and $\beta = 0$.

The correlations for ternary hybrid nanoparticles [48 and 49] are

$$\rho_{\mathrm{Thnf}} = (1-\varphi_1)\{(1-\varphi_2)[(1-\varphi_3)\rho_f + \varphi_3\rho_3] + \varphi_2\rho_2\} + \varphi_1\rho_1, \tag{13}$$

$$\frac{\mu_f}{(1-\varphi_3)^{2.5}(1-\varphi_2)^{2.5}(1-\varphi_1)^{2.5}}, \quad \frac{K_{hnf}}{K_{nf}} = \frac{K_2 + 2K_{nf} - 2\varphi_1(K_{nf} - K_2)}{K_2 + 2K_{nf} + \varphi_2(K_{nf} - K_2)}, \tag{14}$$

$$\frac{K_{Thnf}}{K_{hnf}} = \frac{K_1 + 2K_{hnf} - 2\varphi_1(K_{hnf} - K_1)}{K_1 + 2K_{hnf} + \varphi_1(K_{hnf} - K_1)}, \quad \frac{K_{nf}}{K_f} = \frac{K_3 + 2K_f - 2\varphi_3(K_f - K_3)}{K_3 + 2K_f + \varphi_3(K_f - K_3)}, \tag{15}$$

$$\frac{\sigma_{Tnf}}{\sigma_{hnf}} = \frac{\sigma_1(1 + 2\varphi_1) - \varphi_{hnf}(1 - 2\varphi_1)}{\sigma_1(1 - \varphi_1) + \sigma_{hnf}(1 + \varphi_1)}, \quad \frac{\sigma_{hnf}}{\sigma_{nf}} = \frac{\sigma_2(1 + 2\varphi_2) + \varphi_{nf}(1 - 2\varphi_2)}{\sigma_2(1 - \varphi_2) + \sigma_{nf}(1 + \varphi_2)}, \tag{16}$$

$$\frac{\sigma_{nf}}{\sigma_f} = \frac{\sigma_3(1 + 2\varphi_3) + \varphi_f(1 - 2\varphi_3)}{\sigma_3(1 - \varphi_3) + \sigma_f(1 + \varphi_3)}. \tag{17}$$

Drag force coefficient of Carreau Yasuda liquid is formulated as

$$(\mathrm{Re})^{\frac{1}{2}}C_f = \frac{-\left[\frac{m-1}{d}\mathrm{We}^2(f''(0))^d + 1\right]f''(0)}{(1-\varphi_3)^{2.5}(1-\varphi_2)^{2.5}(1-\varphi_1)^{2.5}}. \tag{18}$$

Rate of heat transfer in the presence of tri-hybrid nanoparticles is

$$(\mathrm{Re})^{-0.5}\,\mathrm{Nu} = -\frac{k_f}{k_{\mathrm{Thnf}}}\theta'(0). \tag{19}$$

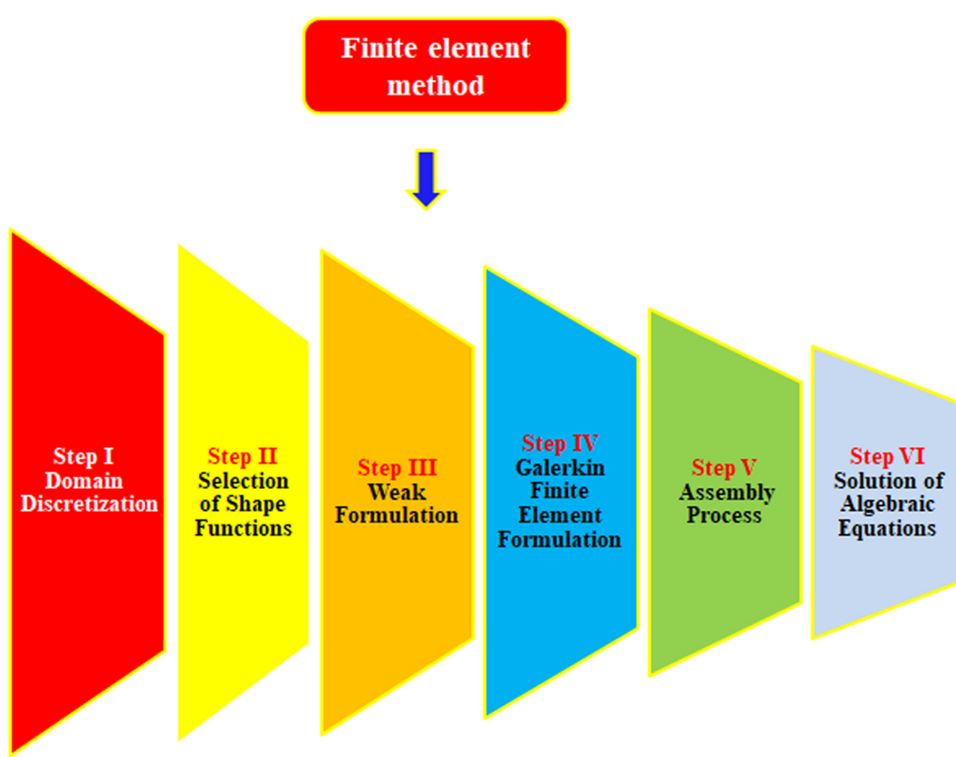

Figure 3: Steps related to FEM.

3 Finite element approach

A strong numerical approach based on FEM is implemented to simulate numerical results of ODEs along with boundary conditions. An FEM is used to conduct the solutions of various CDD problems. It has the capacity to handle complex geometries as well as various types of boundary conditions. Six steps of FEMs are discussed below, while six steps are mentioned in Figure 3. An FEM is observed as a good method in view of accuracy analysis, convergence analysis and stability analysis rather than other numerical methods. The following advantages of implementing FEM are as follows.

- Numerous applications of FEM are investigated in computational fluid mechanics problems;
- Complex types of geometries are tackled by FEM;
- Physical problems based on applied science are developed by FEM;
- It has the ability to discretize the derivatives with very ease;
- An important role of FEM is to solve various types of boundary conditions;
- FEM requires low investment and time rather than other numerical techniques.

Step I: Domain discretization

The first step is about domain discretization of problem domain. Domain is broken into small elements of up to 300 elements. Three hundred elements are enough to simulate the solution of current analysis. It is noticed that a system of ODEs is called strong form, whereas weak form is achieved *via* the residual method.

Step II: Selection of shape function

A significant role of shape functions is used to obtain approximation solution of current analysis. Various types of shape functions are used in finite element procedure. In this procedure, linear kind of shape functions is used. The desired form of shape functions is defined as

$$\psi_j = (-1)^{j-1}\left(\frac{-\eta + \eta_{j-1}}{-\eta_j + \eta_{j+1}}\right), \; i = 1, \; 2. \tag{20}$$

Step III: Weak formulation

Eqs. (12)–(14) are known as strong form along with boundary conditions. In this procedure, weak forms are needed to achieve approximation solution. Collection of all terms is placed on one side and integrated over 300 elements. The desired residuals of present problems are derived as

$$\int_{\eta_e}^{\eta_{e+1}} w_1(F' - S)\mathrm{d}\eta = 0, \tag{21}$$

$$\int_{\eta_e}^{\eta_{e+1}} w_2\left[S'' + (We)^d\frac{(m-1)(d+1)}{d}S''(S')^d - \frac{\nu_{\mathrm{Thnf}}}{\nu_f}\left(S^2 + fS' - \frac{\theta\rho_f 2\beta}{(\eta+\gamma)^4}\right)\right]\mathrm{d}\eta = 0, \tag{22}$$

$$\int_{\eta_e}^{\eta_{e+1}} w_3\left[\begin{array}{l}\theta'' + \dfrac{(\rho C_p)_{\mathrm{THnf}}k_f}{(\rho C_p)_f k_{\mathrm{Thnf}}}[f\theta' - 2S\theta] + \dfrac{(\rho C_p)_{\mathrm{THnf}}k_f}{(\rho C_p)_f k_{\mathrm{Thnf}}}\dfrac{\lambda 2\beta f(\theta-\epsilon)}{(\eta+\gamma)^3}\\ \dfrac{k_f}{k_{\mathrm{Thnf}}}\mathrm{Pr}H_t\theta + \dfrac{k_f}{k_{\mathrm{Thnf}}}\dfrac{\mathrm{EcPr}(1-\phi_2)^{2.5}}{(1-\phi_1)^{2.5}(1-\phi_3)^{2.5}}(S')^2 + \dfrac{k_f}{k_{\mathrm{Thnf}}}(S')^2\end{array}\right]\mathrm{d}\eta = 0. \tag{23}$$

Step IV: Finite element formulation

In this step, stiffness elements are obtained from current problem. Finally, global stiffness matrices are achieved over each element. The stiffness elements are derived as

$$K_{ij}^{13} = 0, K_{ij}^{11} = \int_{\eta_e}^{\eta_{e+1}}\left(\frac{\mathrm{d}\psi_j}{\mathrm{d}\eta}\psi_i\right)\mathrm{d}\eta, \quad K_{ij}^{12} = \int_{\eta_e}^{\eta_{e+1}}(\psi_j\psi_i)\mathrm{d}\eta, \; B_i^1 = 0, \tag{24}$$

$$K_{ij}^{22} = \int_{\eta_e}^{\eta_{e+1}}\left[\begin{array}{l}-\dfrac{\mathrm{d}\psi_i}{\mathrm{d}\eta}\dfrac{\mathrm{d}\psi_j}{\mathrm{d}\eta} - (\mathrm{We})^d\dfrac{(m-1)(d+1)}{d}(\overline{S'})^d\dfrac{\mathrm{d}\psi_i}{\mathrm{d}\eta}\dfrac{\mathrm{d}\psi_j}{\mathrm{d}\eta}\\ -\dfrac{\nu_{\mathrm{Thnf}}}{\nu_f}\left(\bar{S}\psi_i\psi_j + \bar{f}\psi_i\dfrac{\mathrm{d}\psi_j}{\mathrm{d}\eta}\right)\end{array}\right]\mathrm{d}\eta, \tag{25}$$

$$K_{ij}^{21} = 0, \; K_{ij}^{23} = \int_{\eta_e}^{\eta_{e+1}} -\left(\frac{\nu_{\mathrm{Thnf}}}{\nu_f}\frac{\theta\rho_f 2\beta}{(\eta+\gamma)^4}\right)\mathrm{d}\eta, \quad B_i^2 = 0, K_{ij}^{31} = 0, \; B_i^3 = 0, \tag{26}$$

$$K_{ij}^{33} = \int_{\eta_{e+1}}^{\eta_e}\left[\begin{array}{l}-\dfrac{\mathrm{d}\psi_i}{\mathrm{d}\eta}\dfrac{\mathrm{d}\psi_j}{\mathrm{d}\eta} + \dfrac{k_f(\rho C_\mathrm{p})_{\mathrm{THnf}}}{(\rho C_\mathrm{p})_f k_{\mathrm{Thnf}}}\left[\bar{f}\psi_i\dfrac{\mathrm{d}\psi_j}{\mathrm{d}\eta}\right.\\ \left.-2\bar{S}\psi_i\psi_j\right] + \dfrac{k_f}{k_{\mathrm{Thnf}}}\mathrm{Pr}H_t\psi_i\psi_j\\ +\dfrac{(\rho C_\mathrm{p})_{\mathrm{THnf}}k_f}{(\rho C_\mathrm{p})_f k_{\mathrm{Thnf}}}\dfrac{\lambda 2\beta f(-\epsilon)}{(\eta+\gamma)^3}\psi_i\psi_j\end{array}\right]\mathrm{d}\eta, \tag{27}$$

$$K_{ij}^{32} = \int_{\eta_{e+1}}^{\eta_e}\left(\frac{k_f}{k_{\mathrm{Thnf}}}\frac{4\lambda(1-\phi_2)^{2.5}}{(1-\phi_1)^{2.5}(1-\phi_3)^{2.5}}\overline{S'}\psi_i\frac{\mathrm{d}\psi_j}{\mathrm{d}\eta} + \frac{k_f}{k_{\mathrm{Thnf}}}\overline{S'}\psi_i\frac{\mathrm{d}\psi_j}{\mathrm{d}\eta}\right)\mathrm{d}\eta. \tag{28}$$

Step V: Assembly process

Assembly process is an integral part of FEM. Stiffness matrices are formulated using concept of assembly approach.

Step VI: Solution of algebraic equations

Finally, a system of linear algebraic equations is numerically solved within computational tolerance (10^{-5}). The stopping condition is listed below. Flow chart of finite element procedure is given in Figure 4. Furthermore, validation of numerical results in terms of Nusselt number is shown in Table 3. Moreover, programming of FEM is designed on MAPLE 18. Homemade code regarding FEM is developed using MAPLE 18, whereas this code is tested with already published studies.

$$\left|\frac{\delta_{i+1}-\delta_i}{\delta^i}\right| < 10^{-5}. \tag{29}$$

Table 2: Simulations of temperature and velocity at mid of each 300 elements [47,49]

Number of elements	$f'\left(\frac{\eta_\infty}{2}\right)$	$\theta\left(\frac{\eta_\infty}{2}\right)$
30	0.3830450314	0.3240812858
60	0.3833760528	0.2922311857
90	0.3831603611	0.2819022485
120	0.3829500648	0.2768517260
150	0.3827836469	0.2738692845
180	0.3826538369	0.2719045859
210	0.3825512827	0.2705127850
240	0.3824686218	0.2694762872
270	0.3824008552	0.2686761587
300	0.3823104321	0.2683721231

3.1 Mesh-free study

The convergence of problem is investigated through investigation of mesh-free. It is noticed that the present problem becomes grid independent by observing 300 elements. The outcomes of velocity and temperature profiles against 30–300 elements are recorded in Table 2. The convergence of problem is achieved by observing 300 elements. It is included that numerical as well as graphical study is simulated *via* 300 elements.

3.2 Validation of numerical results

Table 3 is prepared to investigate the numerical results of present problem with already published work [46] considering $\mathrm{Ec} = H_t = \lambda = \gamma = \beta = 0$. It is noticed that numerical results of current analysis are simulated by FEM while published results are derived by optimal homotopy analysis method (OHAM) analysis method. It is observed that good comparison is investigated. Moreover, [0, 8] is considered as computational domain and computational

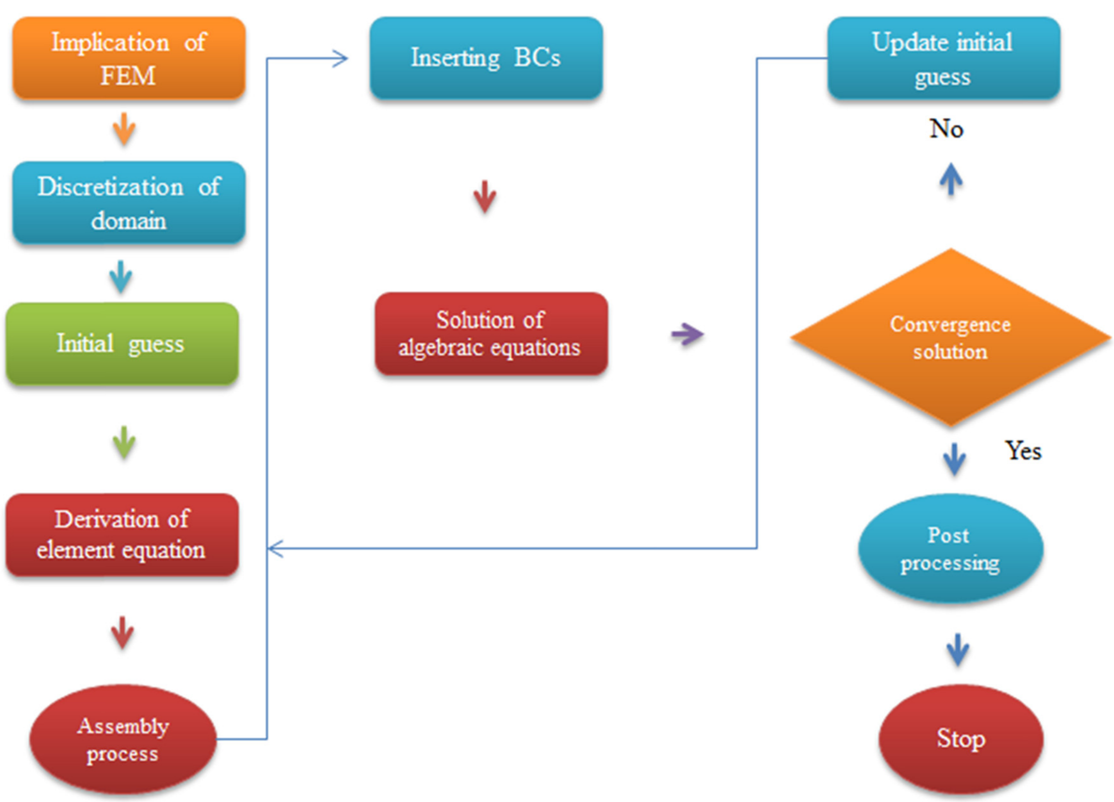

Figure 4: Flow chart *via* FEM.

Table 3: Validation of Nusselt number when $H_t = \lambda = \gamma = \beta = 0$.

Pr	Nadeem *et al.* [46]	Present problem
	OHAM results	FEM results
0.72	0.808641	0.80855192
1.0	1.000000	1.00000000
3.0	1.923690	1.92394013
4.0	2.003170	2.00300358

domain is taken as $\eta_{\max} = 8$ while $\eta_{\max}$ is based on asymptotic boundary conditions where η is satisfied.

4 Results and discussion

A developing model is analyzed inserting heat generation and heat absorption phenomena in Carreau Yasuda martial past a stretching surface. A role of magnetic dipole is implemented toward stretching surface. A viscous dissipation effect is added into heat energy. Such complex-type model is handled with the help of FEM. Graphical simulations and tables are tabulated, whereas graphical discussion of heat energy and velocity fields versus physical parameters is listed below. Here, base fluid is considered as engine oil in ternary hybrid nanofluid. Numerical value of Prandtl fluid [50] is taken as Pr = 6,450.

4.1 Graphical simulations of velocity field

A variation in β, We and m is observed against velocity curves inserting ternary hybrid nanomaterials, whereas these simulations are noticed by Figures 5–7. Figure 5 is prepared to notice variation in velocity curves versus the implication of β. A role of β appeared because of magnetic dipole, while a magnetic dipole is applied at the surface of wall. It is noticed that a magnetic dipole attracts fluid particles at the surface of wall and this attraction of fluid particles toward magnetic dipole creates frictional force among particles and layers. So, this attraction force is the reason for slow down velocity of fluid particles. Therefore, it is included that velocity curves have decreasing function against implication of β. This graph is studied for a case without dipole and presence of magnetic dipole. It is investigated that ferrohydrodynamic interaction number is a dimensionless parameter. The viscosity of fluid is enhanced when ferrohydrodynamic interaction parameter is increased. Physically, viscous force is produced into motion *via* fluid

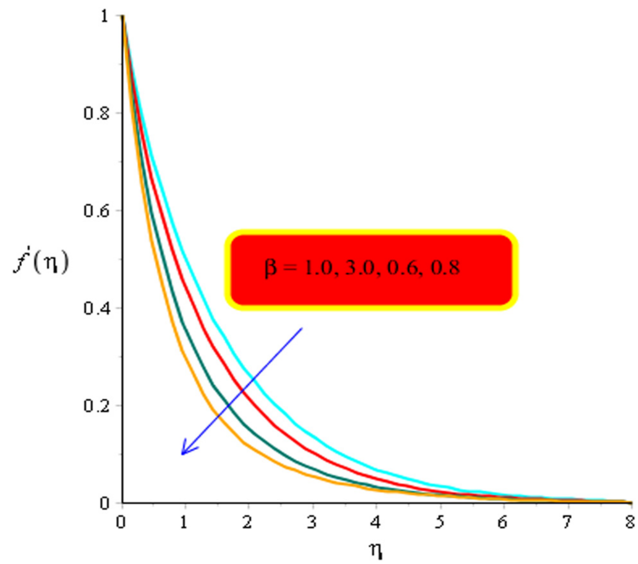

Figure 5: Variation in velocity curves versus β when Pr = 6450, $m = 0.3$, $d = 0.1$, $\lambda = 1.2$, $H_t = -1.3$, $\epsilon = 0.4$, $\gamma = 1.4$, $\varphi_1 = 0.003$, $\varphi_3 = 0.94$, $\varphi_1 = 0.057$, We = 2.0.

particles. Moreover, thermal layer thickness is reduced using argument values of β. An influence of We on velocity curves using ternary hybrid nanoparticles is carried out by Figure 6. Physically, a ratio among viscous force and elastic force makes a Weissenberg number. It is visualized that an increment in We results in increment in viscosity of fluid particles. Hence, fluid becomes significantly vicious when We is increased. Moreover, layers

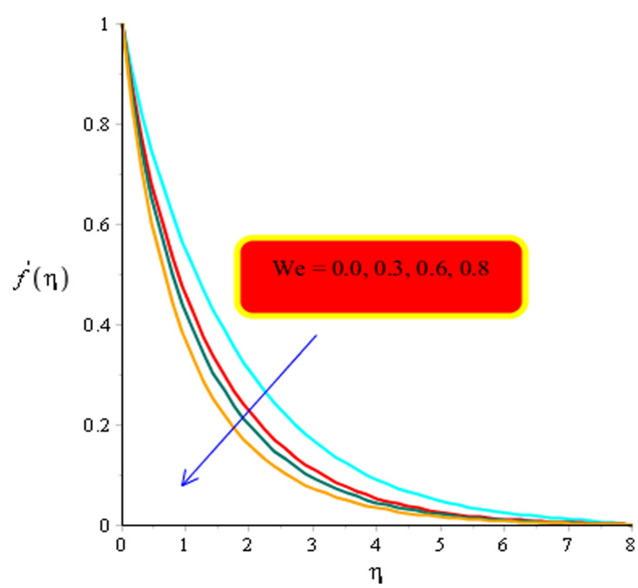

Figure 6: Variation in velocity curves versus We when Pr = 6450, $m = 0.5$, $d = 0.7$, $\lambda = 1.3$, $H_t = 1.5$, $\epsilon = 0.4$, $\gamma = 2.4$, $\varphi_1 = 0.003$, $\varphi_3 = 0.94$, $\varphi_1 = 0.057$, $\beta = 3.0$.

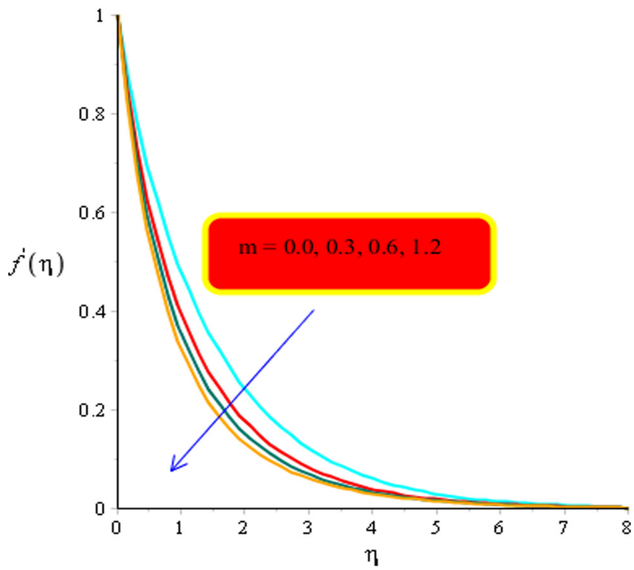

Figure 7: Variation in velocity curves versus m when Pr = 6450, $d = 0.7$, $\beta = 1.3$, $\lambda = 1.2$, $H_t = -1.3$, $\epsilon = 1.4$, $\gamma = 1.4$, $\varphi_1 = 0.003$, $\varphi_3 = 0.94$, , $\varphi_1 = 0.057$, We = 4.0.

of momentum boundary are also decreasing against higher values of We. The Weissenberg number is a dimensionless parameter, which appeared due to occurrence of Carreau Yasuda liquid in the present problem. The present analysis is called non-Newtonian model in the presence of Carreau Yasuda liquid. Figure 7 is plotted to know variation in velocity curves versus implication of power law number. A power law parameter is used to characterize the behavior of fluid category among layers. It is noticed that m is a dimensionless number which appeared due to occurrence of Carreau Yasuda liquid. Momentum boundary layers have less thickness when m is increased. A frictional force is generated among momentum layers, whereas frictional force makes fluid more thick. Furthermore, flow over surface is decreased versus higher values of We

4.2 Graphical simulations of temperature field

Figures 8–11 are plotted to notice the behavior of heat energy versus β, H_t and Ec, while Figure 9 shows the comparison of tri-hybrid nanoparticles, fluid, nanofluid and hybrid nanomaterials. Increase is investigated into heat energy when β is increased. Appearance of β is occurred using the strength of magnetic dipole. A magnetic dipole is used to slow down velocity in particles. It is predicted that higher values of β lead to enhanced thermal energy in fluid particles. This effect occurred due to interaction of magnetic field and nanoparticles. So, a frictional heating phenomenon is enhanced in fluid particles because of interaction of magnetic field in fluid particles. Thickness regarding thermal layers is declined versus argument numerical values of β. Physically, it is a dimensionless parameter which is based on the strength of magnetic dipole. Hence, fluid particles absorbed more heat energy when β is increased. Figure 8 is developed to

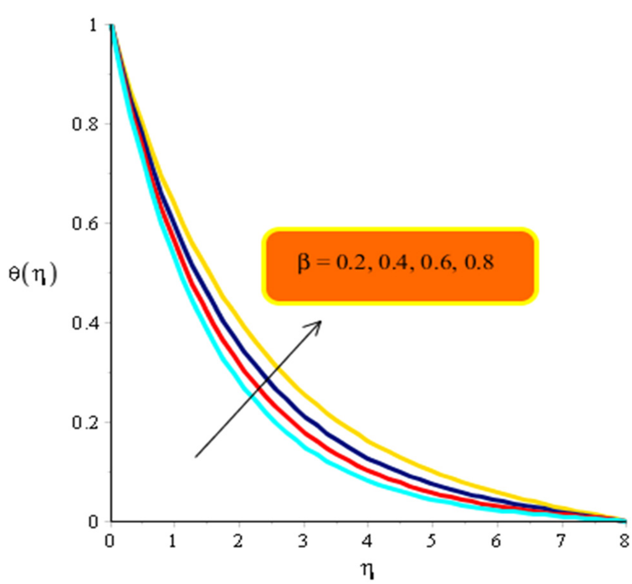

Figure 8: Variation in temperature curves versus β when Pr = 6450, $m = 0.3$, $d = 0.2$, $\beta = 1.7$, $\lambda = 1.2$, $H_t = -1.6$, $\epsilon = 0.4$, $\gamma = 1.4$, $\varphi_1 = 0.003$, $\varphi_3 = 0.94$, $\varphi_1 = 0.057$, We = 3.0.

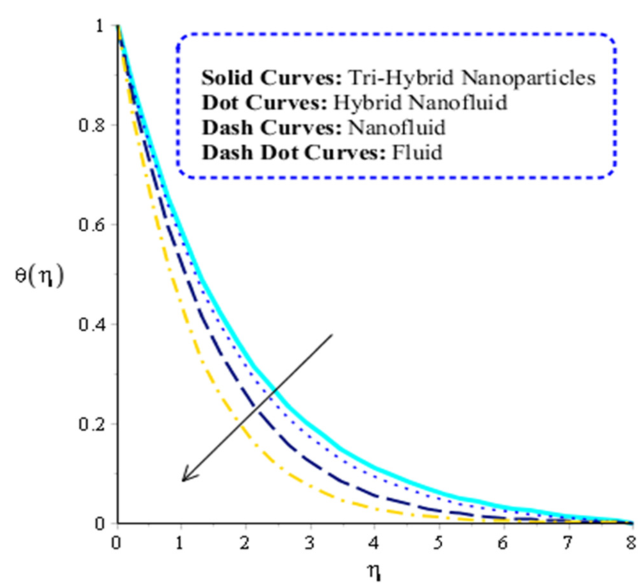

Figure 9: Comparative performance of temperature curves in fluid, hybrid nanofluid, tri-hybrid nanomaterials and hybrid nanofluid.

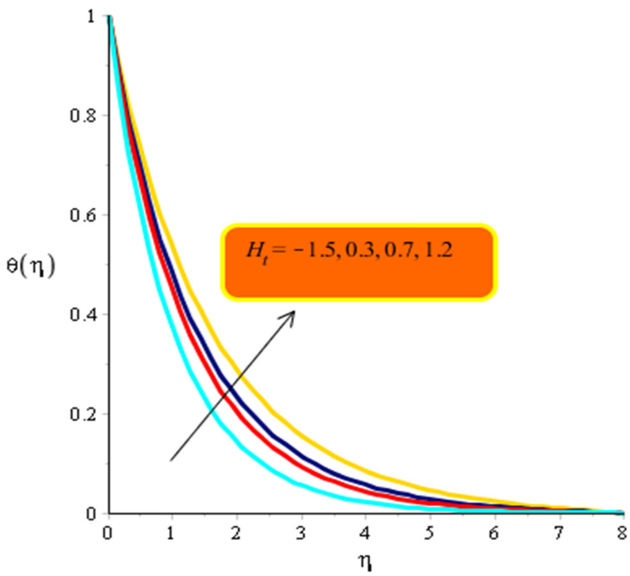

Figure 10: Variation in temperature curves versus H_t when $\varphi_3 = 0.94$, $\varphi_1 = 0.057$, We $= 4.0$. Pr $= 6450$, $m = 0.3$, $d = 0.3$, $\beta = 1.3$, $\lambda = 4.2$, $\epsilon = 0.4$, $\gamma = 1.4$, $\varphi_1 = 0.003$.

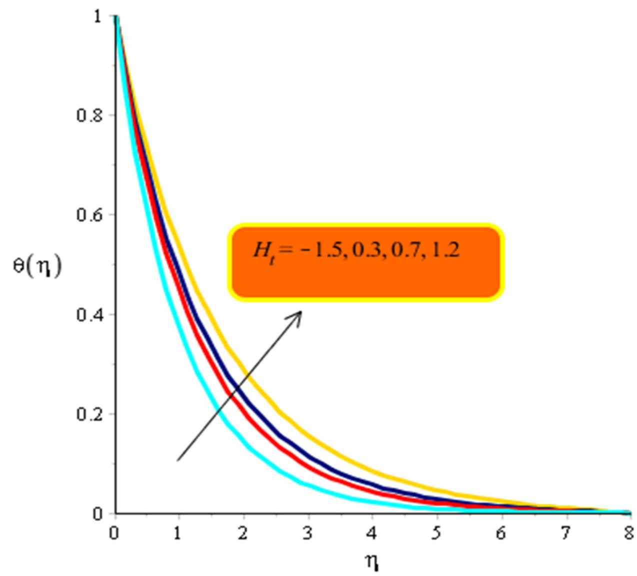

Figure 11: Variation in temperature curves versus Ec when $\varphi_3 = 0.94$, $\varphi_1 = 0.057$, Pr $= 6450$, $d = 0.1$, $\beta = 1.3$, $\epsilon = 0.4$, $\gamma = 1.4$, $\varphi_1 = 0.003$, $\beta = 1.3$, $H_t = -1.3$, $\epsilon = 0.4$, $\gamma = 1.4$, $\varphi_1 = 0.003$.

characterize thermal energy among fluid layers, hybrid nanoparticles layers, nanofluid layers and tri-hybrid nanofluid layers. Figure 8 is most significant visualization among layers using hybrid nanoparticles, nanofluid and tri-hybrid nanofluid. It is concluded that tri-hybrid nanoparticles (mixture of TiO_2, Al_2O_3 and SiO_2 in engine oil) are observed to be most significant among fluid layers for the development of more heat energy rather than heat energy is manufactured for nanofluid, fluid and hybrid nanofluid. Hence, maximum amount of heat energy is achieved for the case of tri-hybrid nanomaterials. Figure 10 exhibits an effect of heat generation parameter on temperature field. Maximum production in thermal energy is generated when external heat source is implemented at the surface of wall. Physically, it happened due to the occurrence of external heat source. It is noticed that two kinds of heat phenomena occurred based on heat absorption and heat generation. Heat absorption is based on $H_t < 0$, whereas heat generation is based on $H_t > 0$. For both cases, heat energy is augmented by implanted higher values of H_t because external heat source is placed at wall. Basically, viscous dissipation number is observed as dimensionless parameter based on viscous dissipation. In energy equation, viscous dissipation parameter appeared in viscous

Table 4: Numerical aspects of Nusselt number and skin friction coefficient against H_t, β, We, m and λ when $\varphi_3 = 0.94$, $\varphi_1 = 0.057$, We $= 2.0$, Pr $= 6450$, $m = 0.3$, $d = 0.1$

Variation in parameters		$-(\mathrm{Re})^{\frac{1}{2}}C_f$	$-\mathrm{Re}^{-\frac{1}{2}}Nu$
	0.0	0.2620890941	0.6269023682
We	0.5	0.2805125031	0.6150064882
	1.5	0.2983840010	0.6038369770
	−1.5	0.4793868421	0.3524502521
H_t	0.0	0.3864742265	0.2572577431
	0.7	0.1464279369	0.2116707874
	0.1	0.07467530385	0.3641197594
m	0.4	0.1547010729	0.5585388446
	0.7	0.2398573119	0.7083760632
	0.0	0.2619130138	0.7417210656
λ	0.4	0.2614998160	0.6310409286
	0.8	0.2612520196	0.5406326980

dissipation term. So, a directly proportional relation is investigated among heat energy and viscous dissipation number. Hence, large values of viscous dissipation number bring more enhancements in heat energy. An influence of viscous dissipation number on temperature field is shown in Figure 11. Heat energy is boosted against implication of viscous dissipation.

4.3 Aspects of Nusselt number and skin friction coefficient against various parameters

Table 4 is tabulated to sketch the effects of Nusselt number and skin friction coefficient against variation in Weissenberg number, heat source parameter, viscous dissipation number and power law number. From Table 4, it is estimated that flow rate and heat transfer rate are decreased versus higher numerical values of heat source parameter. But flow rate is enhanced when Weissenberg number is increased. The role of power law number is observed as very significant to develop maximum amount of heat transfer rate and flow rate. Moreover, heat transfer rate is declined versus argument numerical values of viscous dissipation number.

5 Final outcomes

Mathematical model of Carreau Yasuda liquid is developed in the presence of magnetic dipole *via* stretching surface. Ternary hybrid nano-structures are used to visualize the thermal performance under heat source sink. A finite element scheme is implemented to conduct numerical consequences *via* flow and temperature profiles. Key remarks are summarized as follows:

- Three hundred elements are ensured for visualization of convergence simulations;
- It is noticed that ternary hybrid nanomaterials are observed as a significant source to conduct maximum inclination into thermal energy rather than hybrid nano-structures and nanofluid;
- Temperature profile is inclined versus the higher values of heat generation and viscous dissipation numbers while thermal layers are also increasing the behavior;
- A vital role of magnetic dipole is examined to raise the production of thermal layers but declination is noticed in flow profile;
- Flow rate and heat transfer rate are declined versus argument numerical values of viscous dissipation parameter but opposite behavior on heat transfer rate and flow is studied versus power law number;
- Heat transfer rate is boosted against higher impact of viscous dissipation.

Funding information: Choonkil Park was supported by Basic Science Research Program through the National Research Foundation of Korea funded by the Ministry of Education, Science and Technology (NRF-2017R1D1A1B04032937).

Author contributions: All authors have accepted responsibility for the entire content of this manuscript and approved its submission.

Conflict of interest: The authors state no conflict of interest.

References

[1] Shah SNA, Shah Z, Hussain M, Khan M. Hazardous effects of titanium dioxide nanoparticles in ecosystem. Bioinorg Chem Appl. 2017;2017:2017.
[2] Khan NS, Zuhra S, Shah Z, Bonyah E, Khan W, Islam S. Slip flow of Eyring-Powell nanoliquid film containing graphene nanoparticles. AIP Adv. 2018;8(11):115302.
[3] Rehman KU, Malik MY, Al-Mdallal QM. Physical aspects of magnetized suspended nanoparticles in a rotatory frame: numerical simulation. Ain Shams Eng J. 2020;11(2):479–87.
[4] Alobaid A, Rehman KU, Andleeb S, Erinle KO, Mahmood A. Capacity assessment of carbon-based nanoparticles in stabilizing degraded soils. J King Saud Univ Sci. 2022;34(1):101716.
[5] Ali U, Malik MY, Alderremy AA, Aly S, Rehman KU. A generalized findings on thermal radiation and heat generation/absorption in nanofluid flow regime. Phys A Stat Mech Appl. 2020;553:124026.
[6] Boarescu PM, Boarescu I, Bocșan IC, Gheban D, Bulboacă AE, Nicula C, et al. Antioxidant and anti-inflammatory effects of curcumin nanoparticles on drug-induced acute myocardial infarction in diabetic rats. Antioxidants. 2019;8(10):504.
[7] Pop NL, Nan A, Urda-Cimpean AE, Florea A, Toma VA, Moldovan R, et al. Chitosan functionalized magnetic nanoparticles to provide neural regeneration and recovery after experimental model induced peripheral nerve injury. Biomolecules. 2021;11(5):676.
[8] Iacoviță C, Fizeșan I, Nitica S, Florea A, Barbu-Tudoran L, Dudric R, et al. Silica coating of ferromagnetic iron oxide magnetic nanoparticles significantly enhances their hyperthermia performances for efficiently inducing cancer cells death In Vitro. Pharmaceutics. 2021;13(12):2026.
[9] Swain K, Mebarek-Oudina F, Abo-Dahab SM. Influence of MWCNT/Fe_3O_4 hybrid nanoparticles on an exponentially porous shrinking sheet with chemical reaction and slip boundary conditions. J Therm Anal Calorim. 2021;147:1–10.

[10] Gul T, Firdous K. The experimental study to examine the stable dispersion of the graphene nanoparticles and to look at the $GO-H_2O$ nanofluid flow between two rotating disks. Appl Nanosci. 2018;8(7):1711–27.
[11] Tassaddiq A, Khan S, Bilal M, Gul T, Mukhtar S, Shah Z, et al. Heat and mass transfer together with hybrid nanofluid flow over a rotating disk. AIP Adv. 2020;10(5):055317.
[12] Shafiq A, Rasool G, Khalique CM, Aslam S. Second grade bioconvective nanofluid flow with buoyancy effect and chemical reaction. Symmetry. 2020;12(4):621.
[13] Nisar KS, Khan U, Zaib A, Khan I, Morsy A. A novel study of radiative flow involving micropolar nanoliquid from a shrinking/stretching curved surface including blood gold nanoparticles. Eur Phys J Plus. 2020;135(10):1–19.
[14] Khan U, Zaib A, Sheikholeslami M, Wakif A, Baleanu D. Mixed convective radiative flow through a slender revolution bodies containing molybdenum-disulfide graphene oxide along with generalized hybrid nanoparticles in porous media. Crystals. 2020;10(9):771.
[15] Waqas H, Khan SU, Hassan M, Bhatti MM, Imran M. Analysis on the bioconvection flow of modified second-grade nanofluid containing gyrotactic microorganisms and nanoparticles. J Mol Liq. 2019;291:111231.
[16] Sohail M, Shah Z, Tassaddiq A, Kumam P, Roy P. Entropy generation in MHD Casson fluid flow with variable heat conductance and thermal conductivity over non-linear bi-directional stretching surface. Sci Rep. 2020;10(1):1–16.
[17] Sohail M, Naz R, Shah Z, Kumam P, Thounthong P. Exploration of temperature dependent thermophysical characteristics of yield exhibiting non-Newtonian fluid flow under gyrotactic microorganisms. AIP Adv. 2019;9(12):125016.
[18] Sohail M, Naz R, Abdelsalam SI. Application of non-Fourier double diffusions theories to the boundary-layer flow of a yield stress exhibiting fluid model. Phys A Stat Mech its Appl. 2020;537:122753.
[19] Sheikholeslami M, Ganji DD, Javed MY, Ellahi R. Effect of thermal radiation on magnetohydrodynamics nanofluid flow and heat transfer by means of two phase model. J Magn Magn Mater. 2015;374:36–43.
[20] Sadat R, Agarwal P, Saleh R, Ali MR. Lie symmetry analysis and invariant solutions of 3D Euler equations for axisymmetric, incompressible, and inviscid flow in the cylindrical coordinates. Adv Differ Equ. 2021;2021(1):1–16.
[21] Mousa MM, Ali MR, Ma WX. A combined method for simulating MHD convection in square cavities through localized heating by method of line and penalty-artificial compressibility. J Taibah Univ Sci. 2021;15(1):208–17.
[22] Ali MR, Baleanu D. New wavelet method for solving boundary value problems arising from an adiabatic tubular chemical reactor theory. Int J Biomath. 2020;13(7):2050059.
[23] Sabir Z, Ali MR, Raja MAZ, Shoaib M, Núñez RAS, Sadat R. Computational intelligence approach using Levenberg–Marquardt backpropagation neural networks to solve the fourth-order nonlinear system of Emden–Fowler model. Eng Computers. 2021;1–17.
[24] Baleanu D, Sadat R, Ali MR. The method of lines for solution of the carbon nanotubes engine oil nanofluid over an unsteady rotating disk. Eur Phys J Plus. 2020;135(10):1–13.
[25] Khan MI, Alzahrani F. Binary chemical reaction with activation energy in dissipative flow of non-Newtonian nanomaterial. J Theor Comput Chem. 2020;19(3):2040006.
[26] Khan MI, Alzahrani F, Hobiny A, Ali Z. Modeling of Cattaneo-Christov double diffusions (CCDD) in Williamson nanomaterial slip flow subject to porous medium. J Mater Res Technol. 2020;9(3):6172–7.
[27] Khan MI, Alzahrani F, Hobiny A. Simulation and modeling of second order velocity slip flow of micropolar ferrofluid with Darcy–Forchheimer porous medium. J Mater Res Technol. 2020;9(4):7335–40.
[28] Khan MI, Hayat T, Waqas M, Alsaedi A. Outcome for chemically reactive aspect in flow of tangent hyperbolic material. J Mol Liq. 2017;230:143–51.
[29] Hayat T, Tamoor M, Khan MI, Alsaedi A. Numerical simulation for nonlinear radiative flow by convective cylinder. Results Phys. 2016;6:1031–5.
[30] Khan MI, Qayyum S, Kadry S, Khan WA, Abbas SZ. Irreversibility analysis and heat transport in squeezing nanoliquid flow of non-Newtonian (second-grade) fluid between infinite plates with activation energy. Arab J Sci Eng. 2020;45(6):4939–47.
[31] Wang J, Khan MI, Khan WA, Abbas SZ, Khan MI. Transportation of heat generation/absorption and radiative heat flux in homogeneous–heterogeneous catalytic reactions of non-Newtonian fluid (Oldroyd-B model). Computer Methods Prog Biomed. 2020;189:105310.
[32] Qayyum S, Khan MI, Hayat T, Alsaedi A. Comparative investigation of five nanoparticles in flow of viscous fluid with Joule heating and slip due to rotating disk. Phys B Condens Matter. 2018;534:173–83.
[33] Hayat T, Ahmad S, Khan MI, Alsaedi A. Simulation of ferromagnetic nanomaterial flow of Maxwell fluid. Results Phys. 2018;8:34–40.
[34] Bhatti MM, Alamri SZ, Ellahi R, Abdelsalam SI. Intra-uterine particle–fluid motion through a compliant asymmetric tapered channel with heat transfer. J Therm Anal Calorim. 2021;144(6):2259–67.
[35] Bhatti MM, Abdelsalam SI. Thermodynamic entropy of a magnetized Ree-Eyring particle-fluid motion with irreversibility process: a mathematical paradigm. ZAMM-J Appl Math Mech/Zeitschrift für Angew Math und Mech. 2021;101(6):e202000186.
[36] Elkoumy SR, Barakat EI, Abdelsalam SI. Hall and transverse magnetic field effects on peristaltic flow of a Maxwell fluid through a porous medium. Glob J Pure Appl Math. 2013;9(2):187–203.
[37] Abdelsalam SI, Velasco-Hernández JX, Zaher AZ. Electro-magnetically modulated self-propulsion of swimming sperms *via* cervical canal. Biomech Modeling Mechanobiol. 2021;20(3):861–78.
[38] Eldesoky IM, Abdelsalam SI, El-Askary WA, Ahmed MM. The integrated thermal effect in conjunction with slip conditions on peristaltically induced particle-fluid transport in a catheterized pipe. J Porous Media. 2020;23(7):695–713.
[39] Bhatti MM, Abdelsalam SI. Bio-inspired peristaltic propulsion of hybrid nanofluid flow with Tantalum (Ta) and Gold (Au) nanoparticles under magnetic effects. Waves Random Complex Media. 2021;1–26.
[40] Mekheimer KS, Abo-Elkhair RE, Abdelsalam SI, Ali KK, Moawad AMA. Biomedical simulations of nanoparticles drug delivery to blood hemodynamics in diseased organs: Synovitis problem. Int Commun Heat Mass Transf. 2022;130:105756.

[41] Kalaivanan R, Ganesh NV, Al-Mdallal QM. Buoyancy driven Flow of a Second-Grade nanofluid flow taking into account the Arrhenius activation energy and elastic deformation: models and numerical results. Fluid Dynam Mater Process. 2021;17(2):319–32.
[42] Ganesh NV, Qasem AM, Kalaivananc R. Exact solution for heat transport of Newtonian fluid with quadratic order thermal slip in a porous medium. Adv Theory Nonlinear Anal Appl. 2021;5(1):39–48.
[43] Ganesh NV, Al-Mdallal QM, Öztop HF, Kalaivanan R. Analysis of natural convection for a Casson-based multiwall carbon nanotube nanofluid in a partially heated wavy enclosure with a circular obstacle in the presence of thermal radiation. J Adv Res. 2021
[44] Ganesh NV, Al-Mdallal QM, Hirankumar G, Kalaivanan R, Chamkha AJ. Buoyancy-driven convection of MWCNT–Casson nanofluid in a wavy enclosure with a circular barrier and parallel hot/cold fins. Alex Eng J. 2022;61(4):3249–64.
[45] Ganesh NV, Kalaivanan R, Al-Mdallal QM, Reena K. Buoyancy driven second grade nano boundary layers over a catalytic surface with reaction rate, heat of reaction and activation energy at boundary. Case Stud Therm Eng. 2021;28:101346.
[46] Nadeem S, Ahmad S, Muhammad N. Analysis of ferrite nanoparticles in liquid. Pramana. 2020;94(1):1–9.
[47] Muhammad N, Nadeem S. Ferrite nanoparticles Ni-$ZnFe_2O_4$, Mn-$ZnFe_2O_4$ and Fe_2O_4 in the flow of ferromagnetic nanofluid. Eur Phys J Plus. 2017;132(9):1–12.
[48] Hou E, Wang F, Nazir U, Sohail M, Jabbar N, Thounthong P. Dynamics of tri-hybrid nanoparticles in the rheology of pseudo-plastic liquid with dufour and soret effects. Micromachines. 2022;2022(13):201.
[49] Wang F, Nazir U, Sohail M, El-Zahar ER, Park C, Thounthong P. A Galerkin strategy for tri-hybridized mixture in ethylene glycol comprising variable diffusion and thermal conductivity using non-Fourier's theory. Nanotechnol Rev. 2022;11(1):834–45.
[50] Ouni M, Ladhar LM, Omri M, Jamshed W, Eid MR. Solar water-pump thermal analysis utilizing copper–gold/engine oil hybrid nanofluid flowing in parabolic trough solar collector: Thermal case study. Case Stud Therm Eng. 2022;30:101756.